CO-Breathing Structure Change and Catalysis for Oxygenate Synthesis from CO/H_2 on Supported $[Ru_6C]$ Clusters: Structural and Chemical Controls by Interstitial Carbido Carbon

Yasuo Izumi,[†,§] Teiji Chihara,[‡] Hiroshi Yamazaki,[‡] and Yasuhiro Iwasawa*[,†]

Department of Chemistry, Graduate School of Science, The University of Tokyo, Hongo, Bunkyo-ku, Tokyo 113, Japan, and The Institute of Physical and Chemical Research, Wako-shi, Saitama 351-01, Japan

Received: July 26, 1993; In Final Form: October 22, 1993[⊕]

Catalysis and structures of supported ruthenium carbido clusters $[Ru_6C(CO)_{16}/(CH_3)]^-$/oxides were investigated in comparison with those of supported non-carbido clusters prepared from $[Ru_6(CO)_{18}]^{2-}$ and traditional ruthenium catalysts prepared from $Ru(NO)(NO_3)_3$. Oxygenate synthesis (methanol, dimethyl ether, and formaldehyde) in CO/H_2 reaction was observed on the supported carbido clusters in contrast to the preferential formation of methane and hydrocarbons on the conventional Ru catalysts and the supported non-carbido clusters. The active structure for oxygenate synthesis crucially depended on the kind of oxides; on basic oxides (MgO and La_2O_3) the cluster of framework was incorporated with surface oxygen atoms and expanded or shrunk under CO/H_2 reaction conditions depending on the CO pressure. The reversible expansion–shrinking of the cluster framework was correlated with the activated CO adsorption (CO breathing-induced structural change). On TiO_2 the $[Ru_6C]$ framework always held a shrunk structure as proved by EXAFS. The expanded clusters showed high selectivities in oxygenate synthesis. The shrunk $[Ru_6C]/TiO_2$ also showed much higher activity than the non-carbido cluster or the traditional catalyst. IR and hydrogen isotope effects suggested the formation of oxygenates through a μ_2-formyl intermediate. The switchover of reaction path from the formation of methane and hydrocarbons to oxygenate synthesis is ascribed to the interstitial carbido carbon which has structural effect like a central spring and electronic effect as a four-electron donor on the behavior of the cluster framework.

Introduction

The catalysis of metal clusters[1,2] and supported metal clusters[3,4] has extensively been studied thus far from chemical interests in the unique metal ensembles as well as from industrial viewpoints of developing new catalytic multimetal systems. However, catalysis characteristic of metal cluster framework or that is not observed on traditional metal catalysts is very rare. In addition, precursor clusters with originally well-defined structures are often converted to ill-defined metal particles or degradated to heterogeneous metal sites by pretreatments or during catalytic reactions. Octahedral carbido clusters of iron, ruthenium, osmium, etc. are in general more stable than $M_3(CO)_{12}$ clusters (M = Fe, Ru, Os) and trigonal prismatic $[M_6C]$ clusters (M = Co, Rh, etc).[5-7] We have reported that ruthenium carbido cluster $[Ru_6C(CO)_{16}(CH_3)]^-$ supported on SiO_2 catalyzes selective ethene hydroformylation to form propanal, keeping the hexamer framework $[Ru_6C]$ under catalytic reaction conditions.[8,9] Recently, we also found that the ruthenium carbido clusters supported on MgO, La_2O_3, TiO_2, ZrO_2, and Al_2O_3 catalyze CO hydrogenation to form oxygenates with good selectivities in contrast to poor catalysis of unusal supported ruthenium catalysts for oxygenate synthesis from CO/H_2.[10] The carbido-cluster framework on MgO was also observed to expand or shrink under CO/H_2 reaction conditions;[11] the structure change occurred reversibly between the shrunk cluster (d_{Ru-Ru} = 0.263 nm) and the expanded cluster (0.287 nm) at 523 K.

In this paper we report the catalysis of ruthenium carbido clusters supported on inorganic oxides for oxygenate synthesis from CO/H_2 and the structural transformation of the supported clusters. The present study is connected to chemical modification of the cluster by the interstitial carbido carbon (promoter effect from inside) and to structural effect of carbido carbon like a central spring, by which the switchover of reaction pattern from the formation of methane and hydrocarbons (CO-dissociative hydrogenation) to oxygenate synthesis (CO-associative hydrogenation).

Experimental Section

The supported cluster catalysts were prepared in a similar way to that described previously.[8,10] The procedure is briefly summarized here. TiO_2 (Degussa P25), ZrO_2 (Soekawa, 99.9%), Al_2O_3 (Degussa alon C), and SiO_2 (Fuji-Davison, silica gel no. 952) were evacuated at 473 K before use as supports. ZnO (Kadox-15) was pretreated at 773 K. MgO and La_2O_3 were prepared from $Mg(OH)_2$ (Soekawa, 99.99%), and $La(OH)_3$ (Soekawa, 99.9%) was prepared by calcination at 773 K. Each pretreated oxide was impregnated with a CH_2Cl_2 solution of the cluster $[BTMA]^+[Ru_6C(CO)_{16}(CH_3)]^-$ (**1**)[12] for 1 h at 290 K in argon (99.9999%), followed by removal of the solvent by evacuation. The catalyst derived from $[Ru_6C(CO)_{16}(CH_3)]^-$ is denoted as $[Ru_6C]$/oxide. The loadings of ruthenium were 3.0 (SiO_2), 2.0 (La_2O_3), 1.8 (MgO), 1.5 (TiO_2, Al_2O_3), and 1.0 wt % Ru(ZnO, ZrO_2). $[BTMA]^+_2[Ru_6(CO)_{18}]^{2-}$ (**2**)[13,14] was also supported in a similar manner to the case of **1** by using purified acetone as a solvent (denoted as $[Ru_6]$/oxide). Conventional Ru catalysts were prepared from aqueous solution of $Ru(NO)(NO_3)_3$, followed by calcination at 673 K and by reduction with H_2 at 673 K (denoted as Ru/oxide). The Ru loadings in these systems were adjusted to the loadings for the corresponding $[Ru_6C]$ systems.

The CO/H_2 reactions were carried out under CO (14.6 kPa) and H_2 (14.6 kPa) in the temperature range 423–623 K in a closed circulating system (dead volume 133 mL) with a U-shaped liquid nitrogen trap. The samples were evacuated at 623 K for activation in situ before use as catalyst. The reaction products CO_2, C_2H_6, C_2H_4, and C_3H_6 were analyzed by a gas chromatograph equipped with a 2-m column of VZ-10. The oxygenated compounds like formaldehyde, dimethyl ether, acetaldehyde, methanol, ethanol, and 2-propanol were analyzed with a 4-m column of dioctyl sebacate, and CH_4 was analyzed with a 2-m

† University of Tokyo.
‡ The Institute of Physical and Chemical Research.
§ Present address: Department of Environmental Chemistry and Engineering, Tokyo Institute of Technology, Nagatsuta, Midori-ku, Yokohama 227, Japan.
⊕ Abstract published in *Advance ACS Abstracts,* December 15, 1993.

0022-3654/94/2098-0594$04.50/0

TABLE 1: Turnover Frequencies (TOF) and Selectivities (S) for the Formation of Each Product of Oxygenates in CO (14.6 kPa) + H_2 (14.6 kPa) Reaction on the Ru Catalysts at 473 (A) and 523 K (B)

	$[Ru_6C(CO)_{16}(CH_3)]^-$ TOF[a]						$[Ru_6(CO)_{18}]^{2-}$ TOF[a]						$Ru(NO)(NO_3)_3$ TOF[a]					
precursor	FA[c]	ME[d]	DM[e]	others[f]	Σ	S^b/%	FA[c]	ME[d]	DM[e]	others[f]	Σ	S^b/%	FA[c]	ME[d]	DM[e]	others[f]	Σ	S^b/%
								(A) 473 K										
MgO	0	0.032	0.023	0	0.055	48	–	–	–	–	–	–	0	0	0	0	0	0
MgO[g]	0	0	0	0	0	0	–	–	–	–	–	–	–	–	–	–	–	–
ZnO	0	0.004	0.004	0.009	0.017	24	–	–	–	–	–	–	–	–	–	–	–	–
La_2O_3	0.17	0.12	0.10	0.04	0.43	92	–	–	–	–	–	–	0	0	0	0	0	0
TiO_2	0.10	0.68	0.50	0.12	1.4	53	0	0.051	0.040	0.060	0.15	27	0	0	0	0	0	0
TiO_2[g]	0.052	0.066	0.052	0.019	0.19	35	–	–	–	–	–	–	–	–	–	–	–	–
ZrO_2	0.060	0.24	0.18	0.058	0.53	53	–	–	–	–	–	–	–	–	–	–	–	–
Al_2O_3	0	0.11	0	0	0.11	34	0	0	0	0.003	0.003	2.3	0	0	0	0.17	0.17	4.2
SiO_2	0.006	0.22	0.14	0	0.37	34	–	–	–	–	–	–	–	–	–	–	–	–
								(B) 523 K										
MgO	0.18	0.24	0.25	0.036	0.70	49	–	–	–	–	–	–	0	0.047	0.052	0.061	0.16	3.0
MgO[g]	0	0.12	0.094	0.023	0.23	10	–	–	–	–	–	–	–	–	–	–	–	–
ZnO	0	0.039	0.051	0.006	0.10	10	–	–	–	–	–	–	–	–	–	–	–	–
La_2O_3	1.1	0.39	0.46	0.11	2.1	49	–	–	–	–	–	–	0	0.15	0.16	0.046	0.36	17
TiO_2	5.1	2.9	2.4	0.61	11.0	44	0.20	0.90	0.91	0.10	2.1	30	0	0.046	0.12	0.12	0.30	13
TiO_2[g]	0.80	0.86	0.72	0.14	2.5	28	–	–	–	–	–	–	–	–	–	–	–	–
ZrO_2	1.2	1.1	0.98	0.092	3.4	39	–	–	–	–	–	–	–	–	–	–	–	–
Al_2O_3	2.7	0.98	0.090	0.073	3.8	27	0.063	0.020	0.058	0.004	0.15	7.1	0	0	0	0.51	0.51	2.1
SiO_2	0.27	0.32	0.15	0	0.74	6.2	–	–	–	–	–	–	–	–	–	–	–	–

[a] 10^{-3} min^{-1}. [b] Total oxygenates mol %. [c] Formaldehyde. [d] Methanol. [e] Dimethyl ether. [f] Other oxygenates were mainly acetaldehyde, ethanol, and propanal. [g] Cluster catalysts were reduced with H_2 at 623 K.

column of 5A molecular sieves. The column temperature was always 353 K. The turnover frequency (TOF) for the supported clusters was calculated assuming 100% dispersion of Ru atoms, and for conventional Ru catalysts it was calculated from H_2 uptake at 290 K.

The Ru K-edge EXAFS (extended X-ray absorption fine structure) spectra were measured in a transmission mode by using the EXAFS facilities installed at a beam line 10B of the Photo Factory in the National Laboratory for High Energy Physics (proposal No. 91012). The EXAFS spectra were taken in an EXAFS cell without contacting air by using a Schlenk transfer technique from a closed circulating system for sample preparation to the cell. The EXAFS analysis was performed by a curve-fitting method on the basis of the formula of plane-wave single scattering theory,[15] using empirical phase shift and amplitude functions extracted from cluster **1** for Ru–C(carbonyl) and Ru-(–C–)Ru bonds, $[RuCl_2(CO)_3]_2$ for Ru(–C–)O bond, RuO_2 powder for Ru–O bond, and Ru powder for Ru–Ru(metallic) bond. The phase shift and amplitude functions for Ru–Ru-(cluster) bond were obtained by subtracting the peak of Ru(–C–)O of $[RuCl_2(CO)_3]_2$ from the superimposing peak of Ru–Ru plus Ru(–C–)O of **1**, taking into account each coordination number. The Fourier transform of the k^3-weighted EXAFS oscillation was carried out over the range 30–140 nm^{-1}. In the curve-fitting analysis the Debye–Waller factors for each coordination shell were fixed to be the same values as those obtained in the analyses for the model compounds $[Ru_6C(CO)_{16}(CH_3)]^-$, $[RuCl_2(CO)_3]_2$, RuO_2, and Ru powder.

FT-IR spectra of the supported clusters were recorded on an FTIR spectrometer (JASCO FTIR-7000) in an IR cell with two NaCl windows (self-supporting disk) combined with a closed circulating system. Support wafers were pretreated at a given temperature in the cell and impregnated by the drop of a CH_2Cl_2 solution of the cluster.

Results

Oxygenate Synthesis on Supported $[Ru_6C(CO)_{16}(CH_3)]^-$ Cluster Catalysts. Catalytic oxygenate synthesis from CO/H_2 was studied under CO (14.6 kPa) and H_2 (14.6 kPa) at 473–623 K. The TOFs and the selectivities for the formation of oxygenated compounds, methanol, formaldehyde, and dimethyl ether, at 473 and 523 K are shown in Table 1. For comparison, the results for the catalysts derived from $[Ru_6(CO)_{18}]^{2-}$ and $Ru(NO)(NO_3)_3$ are also listed in Table 1. The TOFs for $[Ru_6C]$/oxides were larger by 10 (TiO_2) to 36 (Al_2O_3) times at 473 K and 5 (TiO_2) to 25 (Al_2O_3) times at 523 K than those for $[Ru_6]$/oxides. The traditional Ru/oxides (TiO_2 and La_2O_3) showed no activity for the oxygenate synthesis at 473 K and the activity at 523 K was also low. The most active $[Ru_6C]/TiO_2$ produced formaldehyde (20%), methanol (12%), and dimethyl ether (9.6%) at 523 K, and the activity did not decrease over 15 h. The order of the activity of $[Ru_6C]$/oxides for support at 473–523 K was $TiO_2 > Al_2O_3 \gtrsim ZrO_2 \gtrsim La_2O_3 > SiO_2 \simeq MgO > ZnO$.

The supported ruthenium carbido clusters also exhibited higher selectivities to oxygenated compounds than $[Ru_6]$/oxides or the conventional ruthenium catalysts (Table 1). Particularly the traditional Ru/oxide catalysts made no sense in practice; the selectivities at 523 K were as low as 17% (La_2O_3), 13% (TiO_2), 2.1% (Al_2O_3), and 3.0% (MgO) against 49, 44, 27, and 49%, respectively, for the corresponding $[Ru_6C]$/oxide catalysts. Among supported carbido clusters, $[Ru_6C]/La_2O_3$ was most selective (92% at 473 K and 49% at 523 K). The order of the selectivity for support was $La_2O_3 > MgO \simeq TiO_2 \gtrsim ZrO_2 > Al_2O_3 > SiO_2 \gtrsim ZnO$. The $[Ru_6C]$/oxide catalysts preferentially produced the oxygenated compounds, while the conventional Ru catalysts produced mainly methane and hydrocarbons (ethene, ethane, and propene). Even if various amounts of carbon were deposited on the metallic Ru particles of Ru/oxide by the Boudouard reaction ($2CO \rightarrow C + CO_2$), the oxygenate synthesis was not augmented. By carbon deposition the reaction rate monotonously decreased due to the partial cover of Ru surface. The TOF for $[Ru_6]/Al_2O_3$ without the interstitial carbon was low enough as compared with conventional impregnated catalysts, probably due to the degradation of the $[Ru_6]$ framework by the reaction with surface oxygen (see hereinafter).

After the reduction of $[Ru_6C]$/MgO and $[Ru_6C]/TiO_2$ in hydrogen at 623 K the catalytic activities for oxygenate synthesis decreased to 0 (473 K) to 32% (523 K) or 13 (473 K) to 22% (523 K) of those before the treatment for $[Ru_6C]$/MgO or $[Ru_6C]/TiO_2$, respectively (Table 1). The TOF and selectivity for $[Ru_6C]/TiO_2$ reduced at 623 K are nearly the same as those for $[Ru_6]/TiO_2$ derived from $[Ru_6(CO)_{18}]^{2-}$.

The rates of oxygenate synthesis were also measured at low CO pressure (0.10 kPa of CO and 29.3 kPa of H_2) at 523 K on $[Ru_6C]$/MgO and $[Ru_6C]/La_2O_3$. The TOFs were only 10–17% of those for the reaction at the pressure of CO (14.6 kPa)

TABLE 2: Turnover Frequencies (10^{-3} min^{-1}) for CO/H_2 and Related Reactions[a]

T_{reac}/K	523		523		473	523		523	
P_{CO}/kPa	14.6		0.10		14.6	14.6			
P_{H_2}/kPa	14.6		29.3		7.3	14.6		14.6	
P_{D_2}/kPa					7.3				
product	HC	ox	HC	ox	HD	HCO_2[c]	CH_3O[c]	HCO_2[d]	CH_3O[d]
$[Ru_6C(CO)_{16}(CH_3)]^-/Al_2O_3$	10	3.8				1.1	0.91	1.3	0
$[Ru_6(CO)_{18}]^{2-}/Al_2O_3$	2.0	0.15							
$Ru(NO)(NO_3)_3/Al_2O_3$	24	0.51							
$[Ru_6C(CO)_{16}(CH_3)]^-/MgO$	0.70	0.70	0	0.12	7100	30[b]	0	0.53	0
$Ru(NO)(NO_3)_3/MgO$	5.1	0.16			1600				
$Ru_6C(CO)_{16}(CH_3)]^-/La_2O_3$	2.1	2.1	0.93	0.22		33[b]	0	1.2	0
$Ru(NO)(NO_3)_3/La_2O_3$	1.7	0.36							
$[Ru_6C(CO)_{16}(CH_3)]^-/TiO_2$	14	11			4100				
$[Ru_6(CO)_{18}]^{2-}/TiO_2$	4.9	2.1			9900				
$Ru(NO)(NO_3)_3/TiO_2$	2.0	0.30			630				

[a] HC, hydrocarbons; ox, oxygenates. [b] At 473 K. [c] The rate of the increase of species. [d] The rate of the decrease of species.

TABLE 3: Hydrogen Isotope Effects in CO/H_2 Reaction on the Supported $[Ru_6C(CO)_{16}(CH_3)]^-$ Clusters and a Conventional Ruthenium Catalyst[a]

	ν_D/ν_H					
catalyst	CH_4	C_2H_4	C_3H_6	H_2CO	CH_3OH	$(CH_3)_2O$
$[Ru_6C]/TiO_2$	1.1	1.1	1.1	1.9	2.0	2.0
$[Ru_6C]/MgO$	1.1	–[b]	–	1.6	1.5	1.4
$[Ru_6C]/La_2O_3$	1.0	–	–	1.5	1.6	1.4
Ru/MgO	0.9	–	–	–	–	–

[a] Reaction temperature = 523 K; CO, 14.6 kPa; H_2 (or D_2), 14.6 kPa. [b] Not produced or negligible.

(Table 2). The catalytic activities in Table 1 were recovered again after the switch of the reaction gas from CO (0.10 kPa) + H_2 (29.3 kPa) to CO (14.6 kPa) + H_2 (14.6 kPa).

H_2–D_2 Exchange in CO. H_2–D_2 (14.6 kPa, 1:1) exchange rates in CO (14.6 kPa) were observed on $[Ru_6C]$/oxides, $[Ru_6]$/oxides, and impregnated Ru catalysts. The rates at 473 K are listed in Table 2. H_2–D_2 exchange rates were more than 3000 times faster than the rate of oxygenate synthesis on every catalyst.

Hydrogen Isotope Effect and Hydrogen Pressure Dependency in CO/H_2 Reaction on Supported $[Ru_6C(CO)_{16}(CH_3)]^-$ Catalysts. The hydrogen isotope effects for oxygenate synthesis were observed with $[Ru_6C]/TiO_2$, $[Ru_6C]/La_2O_3$, and $[Ru_6C]/MgO$. The ratios of ν_D/ν_H for methanol, dimethyl ether, and formaldehyde were larger than unity (Table 3) (1.4–2.0 (average ~1.7)), indicating an inverse isotope effect. The rates of hydrocarbon formation had negligible hydrogen isotope effects.

The TOF for each product was measured as a function of P_{H_2} (4–28 kPa) at a fixed P_{CO} (=14.6 kPa) at 523 K. The rate on $[Ru_6C]/TiO_2$ was given by a power law expression: $r = aP_{H_2}^x$ (a, constant), where x ranged 0.76–0.99 for formaldehyde, methanol, and dimethyl ether.

In more detail the reaction was expressed by the rate equation: $r = kK_{H_2}P_{H_2}/(1 + K_{H_2}P_{H_2})$, assuming the Langmuir-type adsorption of hydrogen on the $[Ru_6C]$ clusters on MgO. The K_{H_2} was determined to be 0.012–0.045 kPa^{-1} which is comparable to 0.034 kPa^{-1} for the quantitative acetaldehyde formation from the methyl ligand of $[Ru_6C(CO)_{16}(CH_3)]^-/SiO_2$ at 398 K in CO + H_2.[9] The $[Ru_6C]$ clusters on La_2O_3 also exhibited a Langmuir-type dependency on P_{H_2} (K_{H_2} = 0.10–0.13 kPa^{-1}).

In Situ EXAFS Studies of Supported $[Ru_6C(CO)_{16}(CH_3)]^-$ Catalysts in CO + H_2. Upon the reaction between $[Ru_6C(CO)_{16}(CH_3)]^-$ cluster and each oxide surface, the methyl ligand of the cluster reacted with the surface hydroxyl group of MgO and La_2O_3 to form methane at 290 K, whereas for $[Ru_6C(CO)_{16}(CH_3)]^-/SiO_2$, Al_2O_3, or TiO_2 systems no gas desorption was observed at 290 K. The EXAFS spectra for the incipient supported clusters on SiO_2, Al_2O_3, and TiO_2 were almost the same as that for **1**, also indicating simple physisorption of **1** on SiO_2, Al_2O_3, and TiO_2.[8] The methyl ligand of the cluster reacted with the surface OH groups of these supports at 373–473 K in vacuum.

Figure 1a shows the EXAFS oscillation, its Fourier transform, and the curve-fitting analysis for the incipient $[Ru_6C]/MgO$. The best-fit results are listed in Table 4. The decrease in the averaged coordination number (N) of Ru–C (2.8 → 2.1) and Ru(–C–)O bonds (2.5 → 2.2) suggests the release of about two CO ligands per one cluster upon supporting. These CO ligands were trapped as surface formates on MgO (CO + OH(a) → HCOO(a)). The amount of HCOO(a) corresponded to about two CO ligands per one cluster (formate peaks: 2838 (m) and 2732 (w,sh) cm^{-1} for ν_{CH}, 1660 (m), 1623 (s) and 1608 (w,sh) cm^{-1} for $\nu_{as(OCO)}$, and 1382 (m) and 1313 (m) cm^{-1} for $\nu_{s(OCO)}$).[16] The observation of Ru–Ru (0.291 nm, N = 4.1) and Ru(–C–)Ru (0.410 nm, 1.0) assures the retention of the $[Ru_6C]$ structure compared to the XRD crystallographic data of **1** (0.290 nm (N = 4.0) and 0.410 nm (1.0), respectively) (Table 4).

Next, the incipient $[Ru_6C]/MgO$ species were evacuated at 523–623 K. The cluster framework was shrunk as characterized by the decrease of d_{Ru-Ru} from 0.291 to 0.263 nm (Table 4b). The $[Ru_6C]$ cluster unit is suggested to be maintained because of the coordination number of about four (4.2) for Ru-Ru bond (Table 4b). The shrunk cluster did not show the Ru(–C–)Ru bond peak as shown in Table 4. It is known that the intensity of the Ru(–C–)Ru multiple scattering peak is greatly reduced when the $\theta_{Ru-C-Ru}$ angle decreases a little from π for the linear conformation in an octahedral symmetry.[17] The shrunk clusters on MgO and La_2O_3 are suggested to be distorted from an octahedral symmetry. In fact the interstitial carbon was detected as CD_4, which exhibited a peak around 573 K in temperature-programmed reaction in D_2 (Figure 2), while surface carbides C(a) deposited on Ru particles/oxides showed a CD_4 peak around 473 K. The peaks higher than ~610 K (peak maximum ~673 K) may be derived from $[BTMA]^+$ because the carbido and non-carbido Ru_6 clusters which both have the same countercation ($[BTMA]^+$) did show the similar higher peak in Figure 2. The cluster framework on La_2O_3, Al_2O_3, and TiO_2 was also shrunk to the framework with d_{Ru-Ru} = 0.262, 0.263, and 0.261 nm, respectively.

Besides Ru–Ru bonds, in the cases of MgO and La_2O_3 a shoulder peak at the lower distance side of Ru–Ru peak appeared in the Fourier transform (Figure 1b2), which was assigned to Ru–O bond at 0.212 nm (MgO) and 0.209 nm (La_2O_3) by the curve-fitting analysis (Figure 1b3 and Table 4).

Drastic change in EXAFS was observed with the MgO and La_2O_3 systems in catalytic CO + H_2 conditions at 523 K. For the $[Ru_6C]$ cluster on MgO the Ru(–C–)Ru multiple scattering peak around 0.37 nm (phase-shift uncorrected) in the Fourier transform appeared again under CO/H_2 for 1 h at 523 K (Figure 1c2). At first we performed a curve-fitting of the EXAFS oscillation by assuming two waves of Ru–C(carbonyl) and Ru(–C–)O because carbonyl peaks were observed by FTIR. The

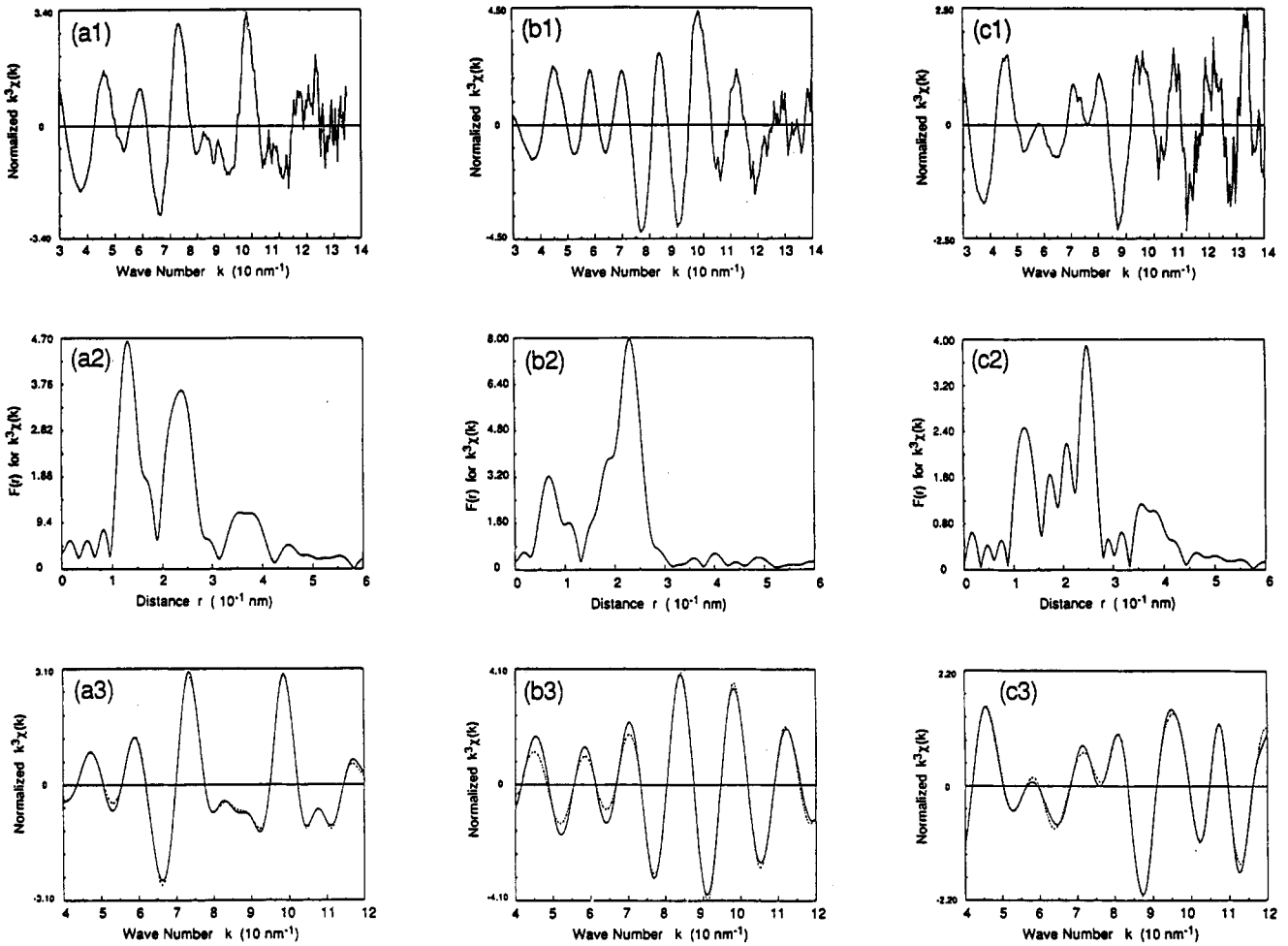

Figure 1. EXAFS spectra for $[Ru_6C(CO)_{16}(CH_3)]^-/MgO$; (a) incipient supported species, (b) after evacuation at 623 K in vacuum, and (c) after CO (14.6 kPa)/H_2 (14.6 kPa) reaction at 523 K for 1 h; (1) k^3-weighted EXAFS oscillation, (2) its associated Fourier transform, and (3) curve-fitting analysis, (—) observed; (- - -) calculated.

TABLE 4: Results of the Curve-Fitting Analysis of Ru K-Edge EXAFS for Supported $[Ru_6C(CO)_{16}(CH_3)]^-$ (A) and $[Ru_6(CO)_{18}]^{2-}$ (B)[a]

	Ru–C			Ru–Ru			Ru(–C–)O			Ru(–C–)Ru[d]			Ru–O			Ru–Ru			
	N	*d*/nm	Δ*E*/eV	*N*	*d*/nm	*E*/eV	*N*	*d*/nm	Δ*E*/eV	*N*	*d*/nm	Δ*E*/eV	*N*	*d*/nm	Δ*E*/eV	*N*	*d*/nm	Δ*E*/eV	R_f[b]/%
SiO_2 (c)				6.6	0.265	−8.4													3.8
Al_2O_3 (b)				4.4	0.263	−3.7													5.8
Al_2O_3 (c)	0.8	0.186	−11	3.8	0.267	−5.5	0.8	0.300	−1.9										3.8
TiO_2 (b)				3.2	0.261	−10													5.3
TiO_2 (c)	0.6	0.184	−7.7	3.5	0.263	−11	0.6	0.299	−10										5.4
MgO (a)	2.1	0.190	−4.5	4.1	0.291	−0.3	2.2	0.301	−1.9	1.0	0.410	0.8							1.7
MgO (b)				4.2	0.263	−3.4							1.1	0.212	3.1				3.2
MgO (c)	(1.4	0.185	−19				1.3	0.306	0.3										12)
	(1.5	0.186	−10	2.3	0.284	−11	1.3	0.305	−1.0										6.2)
	(1.5	0.184	−14	2.2	0.280	−18	1.3	0.306	0.1	0.9	0.409	−0.4							5.2)
	1.6	0.188	−5.8	3.9	0.287	−3.6	1.7	0.299	−4.3	0.8	0.410	0.8	0.8	0.204	4.5				2.6
MgO (d)	1.0	0.187	−7.8	4.2	0.269	−5.5	1.2	0.300	−6.0				0.7	0.211	4.7	1.0	0.381	−6.0	1.7
La_2O_3 (b)				3.3	0.262	−4.8							0.7	0.209	4.5				3.7
La_2O_3 (c)	0.9	0.188	−5.8	3.1	0.277	0.3	0.9	0.301	−1.0				0.5	0.198	0.2				2.2
Al_2O_3 (b)	0.9	0.192	−0.1	1.9	0.261	−3.7	0.7	0.299	−2.7				1.8	0.206	1.4				4.5
TiO_2 (b)				3.8	0.264	−6.4													5.5
XRD*[c]	2.8	0.190		4.0	0.290		2.5	0.302		1.0	0.410								

[a] Debye–Waller factor was taken to be equal to that obtained in the analysis for the model compounds. (a) Incipient supported species; (b), (a) was evacuated at 523–623 K; (c) (b) was treated in CO(14.6 kPa) + H_2(14.6 kPa) at 523 K; and (d) (b) was reduced in H_2(14.6 kPa) at 623 K and treated in CO(14.6 kPa) + H_2(14.6 kPa) at 523 K. [b] Residual factor (= $\int|k^3\chi^{obs}(k) - k^3\chi^{calc}(k)|^2\,dk/\int|k^3\chi^{obs}(k)|^2\,dk$). [c] XRD analysis for $[N(CH_3)_3CH_2Ph]^+[Ru_6C(CO)_{16}(CH_3)]^-$. [d] A multiple scattering shell corresponding to a diagonal line of the octahedral $[Ru_6C]$ framework.

two-wave fitting in Figure 3a did not fit the experimental data at all (R_f 12% in Table 4). Next the three-wave fitting of Ru–C(carbonyl), Ru–Ru, and Ru(–C–)O was conducted in Figure 3b because the shrunk cluster holds the nearest-neighbor Ru–Ru bond. The fitting was improved, but the oscillation in the higher wavenumber region was not reproduced (R_f 6.2% in Table 3). Therefore, the Ru(–C–)Ru bond which should be observed in the octahedral structure of $[Ru_6C]$ was added in the four-wave fitting in Figure 3c, exhibiting a good fit in the higher wavenumber region (R_f 5.2% in Table 3). However, in the curve-fitting of Figure 3c the lower wavenumber oscillation was not reproduced. Since the shrunk $[Ru_6C]$ species were linked to MgO surface

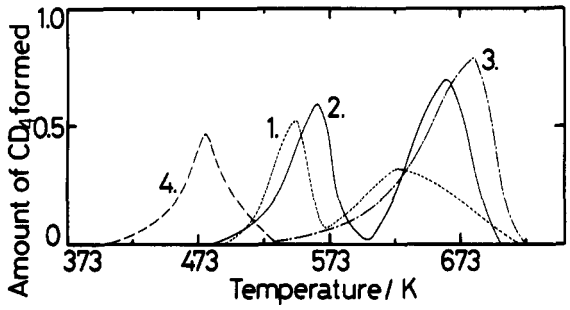

Figure 2. Temperature-programmed reduction spectra in D_2 for (1) $[Ru_6C(CO)_{16}(CH_3)]^-/TiO_2$, (2) $[Ru_6C(CO)_{16}(CH_3)]^-/MgO$, (3) $[Ru_6(CO)_{18}]^{2-}/TiO_2$, (4) C(a)/conventional Ru/MgO. The heating rate 4 k min^{-1}.

through the surface oxygen atoms, we finally performed the five-wave fitting by Ru–C(carbonyl), Ru–Ru, and Ru(–C–)O, Ru(–C–)Ru, and Ru–O_s. Figure 3d shows the best fit with R_f = 2.6%. The Ru(–C–)Ru distance and its coordination number were determined to be 0.410 nm and 0.8, respectively, in Table 3, which are almost the same as those for the original cluster and the incipient $[Ru_6C]/MgO$. The distance of the nearest-neighbor Ru–Ru bond increased from 0.263 to 0.287 nm which is similar to 0.290 nm for the original cluster (XRD).

This expansion of the cluster framework is suggested to be caused by CO adsorption on the $[Ru_6C]$ framework. Table 4 shows the coordination number of 1.6–1.7 for Ru–CO bonds (d_{Ru-C} = 0.188 nm, $d_{Ru(-C-)O}$ = 0.299 nm). The value implies 11 carbonyl ligands per $[Ru_6C]$. The number of CO ligands per cluster determined by CO adsorption and IR intensity for carbonyl peaks is shown in Table 5. These values coincide with the value estimated by EXAFS. The amount of CO adsorption on the shrunk $[Ru_6C]$ clusters on MgO and La_2O_3 was much larger at 523 K than at 290 K, which indicates that the expansion of the cluster framework observed by EXAFS is an activated process induced by CO uptake. For the expanded cluster the bridging CO was observed at 1795 cm^{-1} besides the linear CO peaks at 2045 (w,sh), 1989 (s), and 1933 (w,sh) cm^{-1} for the sample on MgO. The expanded cluster was shrunk again by CO release by evacuation or at a low pressure of CO at 523 K. This expansion–shrink cycle of the $[Ru_6C]$ framework reversibly took place in conjunction with CO breathing.

In the case of the shrunk $[Ru_6C]$ cluster (d_{Ru-Ru} = 0.262 nm) on La_2O_3, the Ru–Ru distance was elongated to 0.277 nm under CO/H_2 reaction conditions. The distance is shorter than 0.287 nm for the case of MgO. Its coordination number was 3.1 which is similar to 3.3 for the shrunk species. The coordination number of Ru–CO bond was 0.9 which is much smaller than 1.6–1.7 for the $[Ru_6C]/MgO$ in Table 4. The incomplete expansion is consistent with the less coordination of CO ligand to ruthenium atom.

In order to examine the behavior of the non-carbido cluster the carbon was removed as CH_4(g) by the treatment with H_2 at 623 K (Figure 2), and then the sample was exposed to CO/H_2 at 523 K. The EXAFS analysis of the obtained sample revealed no significant expansion of the $[Ru_6]$ framework, where the distances and coordination numbers (N) of Ru–Ru and Ru–O bonds were observed at 0.269 nm with N = 4.2 and 0.211 nm with N = 0.7, respectively (Table 4). Besides the nearest-neighbor Ru–Ru at 0.269 nm the next-nearest Ru–Ru bond was observed at 0.381 nm with N = 1.0 (Table 4).

The result for $[Ru_6(CO)_{18}]^{2-}/Al_2O_3$ after evacuation at 623 K indicated that the Ru_6 cluster degradated to small clusters like Ru_3 species (d_{Ru-Ru} = 0.261 nm, N_{Ru-Ru} = 1.9) (Table 4) in contrast to the retention of the framework for $[Ru_6C]/MgO$, La_2O_3, TiO_2, and Al_2O_3.

In Situ Infrared Spectra for Supported $[Ru_6C(CO)_{16}(CH_3)]^-$ Clusters in CO/H_2 Reaction Conditions. The stretching frequencies of carbonyl peaks (adsorbed CO) for the supported clusters and the conventional catalysts are shown in Table 6. The main peaks for the $[Ru_6C]$/oxides were observed at lower frequencies by 97, 58, and 21 cm^{-1} for Al_2O_3, TiO_2, and MgO, respectively, than those for the corresponding conventional Ru catalysts.

In situ IR spectra for supported $[Ru_6C]$ catalysts in CO/H_2 reaction showed formate peaks at 1606 ($\nu_{as(OCO)}$), 1388 ($\nu_{s(OCO)}$), and 1343 cm^{-1} ($\nu_{s(OCO)}$) for $[Ru_6C]/MgO$,[16] at 1580 cm^{-1} ($\nu_{as(OCO)}$) for $[Ru_6C]/La_2O_3$, and at 1592 ($\nu_{as(OCO)}$), 1392 (δ_{CH}), and 1380 cm^{-1} ($\nu_{s(OCO)}$) for $[Ru_6C]/Al_2O_3$.[21,22] On the Al_2O_3 system, methoxy species at 1460 cm^{-1} (δ_{CH}) was also observed.[22] The formation and decomposition rates of formate and methoxy species are shown in Table 2. For the Al_2O_3 system, both rates of the formation and decomposition of formate and methoxy species were smaller than the TOF for oxygenates. In the cases of TiO_2 and La_2O_3 the increase of formates was much faster than the oxygenate synthesis, but the decrease of formates was slower than the oxygenate synthesis (Table 2). These results suggest that the two types of adsorbates have no relation to the catalytic process and are only situated probably on the supports.

The IR peaks in the region 1700–1200-cm^{-1} in CO/H_2 reaction on $[Ru_6C]/TiO_2$ were much weaker than those on $[Ru_6C]/MgO$, $[Ru_6C]/La_2O_3$, or $[Ru_6C]/Al_2O_3$ (Figure 4). This made the observation of reaction intermediate like formyl on Ru possible. We observed a weak peak at 1576 cm^{-1} in CO/H_2 reaction. It shifted to 1551 cm^{-1} immediately after the switch of ambient gas from CO + H_2 to CO + D_2 at 523 K. The peak disappeared very rapidly by the evacuation at 523 K, so that the species at 1576 cm^{-1} is observable only under the reaction conditions. Two peaks at 1619 and 1374 cm^{-1} still remained after the evacuation for 10 min at 523 K which are assigned to formates on TiO_2 surface. The ν_{CO} of formyl and formaldehyde together with the ν_{OCO} of formates on organometallic complexes and catalyst surfaces are listed in Table 7. The 1576-cm^{-1} peak may be assigned to formyl species rather than formates. The similar peaks at 1587 cm^{-1} on Rh/SiO_2[27] and 1584 cm^{-1} on $[RuCo_3]/SiO_2$[28] have been assigned to formyl species (Table 7), which also exhibited H/D-isotope shift as in our case. The peaks at 3020 (2260) and 1306 cm^{-1} are due to methane in gas phase (in parentheses; in CO + D_2, also in the next sentence).[29] The peaks at 2965 (2221), 2877 (2186), 1441 (1427), and 1346 (1332) cm^{-1} can be assigned to methyl, and the peaks at 2929 (2203) and 2856 (2137) cm^{-1} are the ν_{CH} of methylene species.

We observed a weak absorption peak around 1954 cm^{-1} for terminal hydride in H_2 atmosphere (without CO) at 290 K for the $[Ru_6C]/TiO_2$ preheated at 623 K. The peak was replaced by 1430 cm^{-1} in D_2. In the CO/H_2 reaction conditions at 523 K the terminal hydride peak was not observed. Any μ_2-bridging hydride peak was not observed either unlike the observation of μ_2-bridging hydrides on ruthenium clusters.[30-4]

Discussion

It was found that the supported ruthenium carbido clusters preferentially produced methanol, dimethyl ether, and formaldehyde in CO hydrogenation, which is contrasted to the formation of methane and hydrocarbons on conventional Ru catalysts or $[Ru_6(CO)_{18}]^{2-}$-derived catalysts (Table 1). Thus the associative-type hydrogenation of CO without CO dissociation is favorable on the supported carbido clusters, whereas the dissociative-type hydrogenation of CO through CO bond-breaking mainly proceeds on the traditional and non-carbido-cluster catalysts. The catalytic performance of the $[Ru_6C]$ clusters on inorganic oxide supports is connected to the active structure, structural change, and electronic state of the clusters in CO/H_2 reaction conditions hereinafter.

The active structures of the $[Ru_6C]$ clusters on MgO, La_2O_3, TiO_2, Al_2O_3, and SiO_2 under the CO/H_2 reaction conditions were examined by EXAFS. In the case of MgO- and La_2O_3-

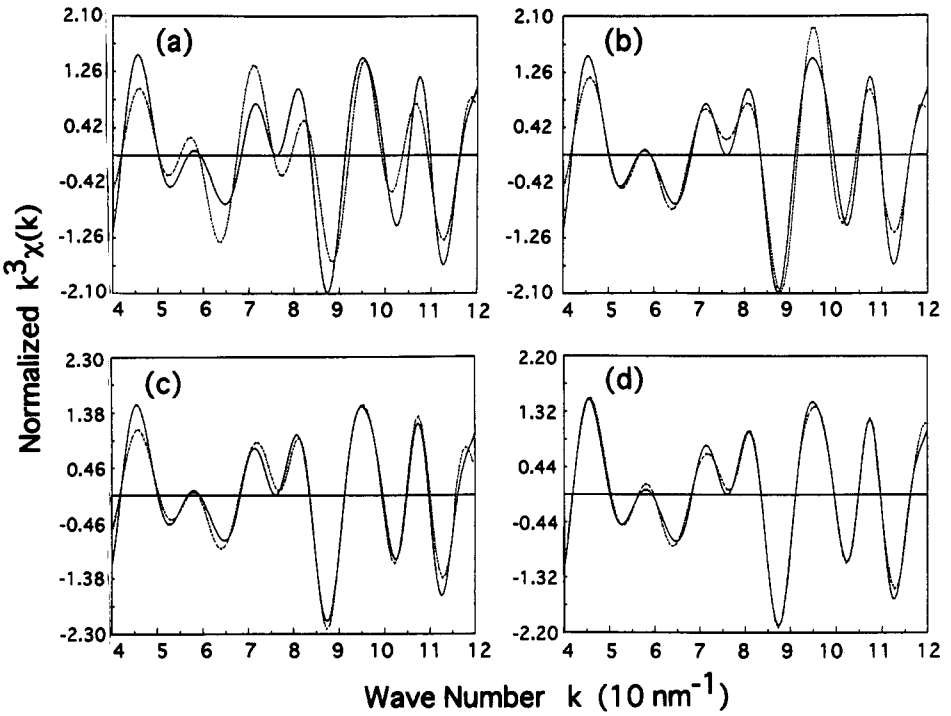

Figure 3. Curve-fitting analyses for inversely Fourier-transformed EXAFS oscillation in Figure 1c; (a) two-wave (Ru–C, Ru(–C–)O) fitting; (b) three-wave (Ru–C, Ru–Ru, Ru(–C–)O) fitting; (c) -four-wave (Ru–C, Ru–Ru, Ru(–C–)O, Ru(–C–)Ru) fitting; and (d) five-wave (Ru–C, Ru–Ru, Ru(–C–)O, Ru(–C–)Ru, Ru–O_s) fitting; (—) observed; (- - -) calculated.

TABLE 5: Amounts of CO Uptake on the Shrunk $[Ru_6C]$ in CO(14.6 kPa) + H_2(14.6 kPa)

	no. of CO per Ru_6C					
	MgO		La_2O_3		TiO_2	Al_2O_3
T/K	290	523	290	523	523	523
CO uptake[a]	2.9	10.7	4.0	7.9	4.0	6.1
IR intensity[b]	3.2	10.6	3.6	8.1	5.8	7.6

[a] Determined taking into account the amount of formates on oxides. [b] Calculated from the ν_{CO} peak area by using the incipient ruthenium carbido cluster as reference.

TABLE 6: IR Absorption Peaks of CO Adsorbed on Supported $[Ru_6C(CO)_{16}(CH_3)]^-$ and $[Ru_6(CO)_{18}]^{2-}$ Clusters and Conventional Ruthenium Catalysts

	ν/cm^{-1}		
precursor	$[Ru_6C(CO)_{16}(CH_3)]^-$ [a]	$[Ru_6(CO)_{18}]^{2-}$ [a]	Ru salt
Al_2O_3	2040 (m,sh)	2143 (w)	2137 (w)[c,d]
	1976 (s)	2054 (m,sh)	2073 (s)
	1752 (w,br)	1978 (s)	2050 (m,sh)
TiO_2	2072 (m,sh)	2139 (m)	2140 (m)[c,e]
	2002 (s)	2074 (s)	2085 (w,sh)
	1975 (w,sh)	2042 (s,sh)	2060 (s)
		2006 (w,sh)	
MgO	2045 (w,sh)		2010 (s,br)[b,f]
	1989 (s)		
	1933 (w,sh)		
	1795 (w,br)		

[a] In CO + H_2 at 523 K. [b] In CO + H_2 at 548 K. [c] In CO at room temperature. [d] From $RuCl_3$ (d_{ave} = 1.4 nm).[18] [e] From $Ru(NO_3)_3$ (d_{ave} = 3.0 nm).[19] [f] From $RuCl_3$.[20]

supported system the incipient $[Ru_6C]$ cluster was incorporated with surface oxygen atoms by evacuation at 523–623 K (Table 4b, and Figure 1b). The bond distance of Ru–O_s were similar to others recently reported.[35-39] The surface oxygen(O_s)-incorporated structures $[Ru_3(\mu\text{-}O_s)_3]$ or $[Ru_3(CO)_6(\mu\text{-}O_s)_3]$ have been proposed for $[Ru_3(CO)_{12}]MgO$.[36,37] Upon supporting, one CH_3 and two CO ligands per cluster were lost, which implies the advantageous interaction between a cluster face composed of three ruthenium atoms and support surface. In an octahedral

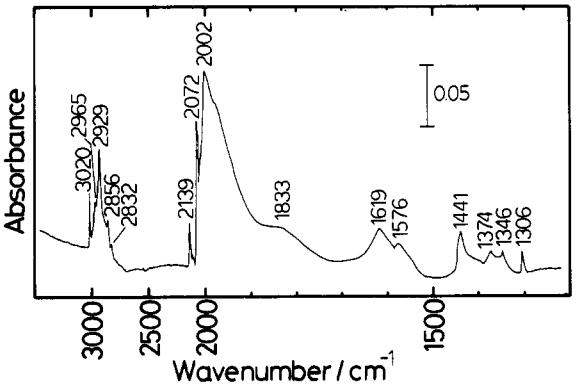

Figure 4. In situ FT-IR spectrum of $[Ru_6C(CO)_{16}(CH_3)]^-/TiO_2$ in CO (14.6 kPa) and H_2 (14.6 kPa) at 523 K (after 40 min).

structure of the cluster the opposite face to the face attached to the surface cannot interact with the surface. The coordination number of Ru–O_s bond was determined to be about unity (1.1 (MgO) and 0.7 (La_2O_3); Table 4b), suggesting that each ruthenium atom of the bottom face directly attached to the surface is bonded to two oxygen atoms because the EXAFS coordination number is of averaged one for total Ru atoms of a cluster. From these results we propose the $[Ru_6C(\mu\text{-}O_s)_3]$ cluster structure with three bridging oxygen atoms incorporated from the surface as shown in Figure 5b.

In the catalytic CO/H_2 conditions the surface-attached $[Ru_6C(\mu\text{-}O_s)_3]$ species showed activated CO adsorption at 523 K (~11 and ~8 CO/$[Ru_6C]$ on MgO and La_2O_3, respectively, compared to 3–4 CO/$[Ru_6C]$ at 290 K, as shown in Table 5. This CO adsorption caused the expansion of the $[Ru_6C]$ framework as proved by the observation of the multiple scattering Ru(–C–)Ru peak (0.410 nm, N = 0.8; Table 4c and Figure 1c) and the elongation of the nearest Ru–Ru bond (0.287 nm, N = 3.9; Table 4c) on MgO. We conducted the systematic curve-fitting analyses with two, three, four, and five waves for the expanded species (Table 4; MgO-c) as described above. Only the five-wave analysis reproduced the observed EXAFS data with a convincing reliability over a whole wavenumber region (Figure 3). The EXAFS analysis

TABLE 7: IR Absorption Peaks of Formyl and Formaldehyde Ligands in Organometallic Compounds and Formyl Adsorbed on Catalyst Surface

species	wavenumber/cm^{-1} ν_{CH}	ν_{CO}	$\nu_{CO_2}^{as}$	$\nu_{CO_2}^{s}$	ref
$Os(CHO)H(CO)_2(PPh_3)_2$	2760 w, 2680 w, 2540 m	1601			23
$Os(CHO)Cl(CO)_2(PPh_3)_2$	2620 w, 2540 w	1610 s			24
$Na^+[Fe(CHO)(CO)_4]^-$	2690, 2540	1577			25
$[Et_4N]^+[Fe(CHO)(CO)_3(P(OPh)_3)]^-$	2515 w	1584 m			26
$Os(\eta^2\text{-}CH_2O)(CO)_2(PPh_3)_2$	2910 w, 2820 m	1017 m			23
CHO(a)/Rh/SiO_2		1587 (1545)			27
CHO(a)/[$RuCo_3$]/SiO_2		1584 (1575)			28
CHO(a)/[Ru_6C]/TiO_2		1576 (1551)			this work

[a] The values in parentheses are for deuterium-labeled species.

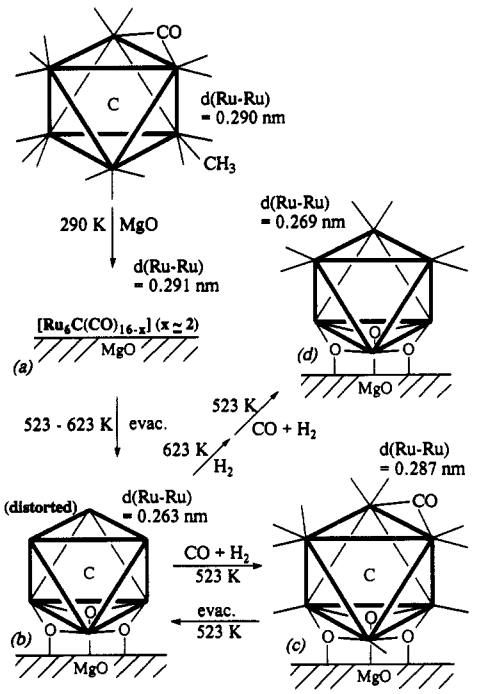

Figure 5. Structure transformation of $[Ru_6C(CO)_{16}(CH_3)]^-$/MgO including reversible expansion–shrink of the cluster framework.

indicates the recovery of a nearly ideal octahedral metal framework for $[Ru_6C(CO)_{11}(\mu\text{-}O_s)_3]$/MgO by CO uptake at 523 K (Figure 4c) and the shrinking of the cluster structure by CO release. The expansion and shrinking of the structure was reversible on MgO (d_{Ru-Ru} = 0.263–0.287 nm). Similar but incomplete expansion–shrink cycle of [Ru_6C] was observed on La_2O_3 (d_{Ru-Ru} = 0.262 ⇄ 0.277 nm; Table 4; La_2O_3). The supported clusters like [Ru_6C]/MgO and [Ru_6C]/La_2O_3 which exhibit a reversible expansion–shrink cycle are classified as "type I".

On TiO_2 and Al_2O_3 the EXAFS spectra after evacuation at 523–623 K were simply fitted with one wave of the nearest Ru–Ru bond (Table 4; TiO_2-b, Al_2O_3-b). There is no evidence of Ru–O_s bond on TiO_2 and Al_2O_3. These [Ru_6C] species on TiO_2 and Al_2O_3 hardly expand in the CO/H_2 conditions (Table 4) and are classified as "type II". The six-Ru unit aggregated to be the species which shows the N_{Ru-Ru} of 6.6 (classified as "type III").

The expansion–shrink of cluster framework induced by CO breathing was observed with the supported clusters which have the interstitial carbido carbon and are incorporated by surface oxygen atoms of MgO or La_2O_3 (basic oxides). The surface oxygen incorporated to the cluster seems important in the reversible transformation of shrunk $[Ru_6C(\mu\text{-}O_s)_3]$ ⇄ expanded $[Ru_6C(CO)_{11}(\mu\text{-}O_s)_3]$ on MgO. In the previous reports for $[Os_{10}C(CO)_{24}]^{x-}$/MgO,[40] $[Pd_{13}(CO)_x]$/NaY,[41] or $[Rh_6(CO)_{16}]$/Al_2O_3,[3] the contribution of oxide surfaces was unclear.

The interstitial carbido carbon has structural and electronic effects on the cluster framework in the specific oxygenate synthesis. The [Ru_6C]/Al_2O_3 and /TiO_2 hold the [Ru_6C] structure in CO/H_2 conditions (type II), whereas the [Ru_6]/Al_2O_3 derived from $[Ru_6(CO)_{18}]^{2-}$ without carbido carbon degradated to $[Ru_3(CO)_3(\mu\text{-}O)_3]$[36,37] as suggested by EXAFS (Table 4). The reversible structure change of [Ru_6C] on MgO and La_2O_3 depending on the CO pressure (type I) indicates thermodynamical stability of the carbido cluster because other non-carbido Ru clusters never showed such phenomenon. The [Ru_6]/MgO obtained by removal of the interstitial carbon atom with H_2 reduction showed only a little change of Ru–Ru bond (0.263 → 0.269 nm) compared with the large expansion from 0.263 → 0.287 nm for the [Ru_6C]/MgO. These results demonstrate that the interstitial carbon has a key role like a central spring to make the cluster structure flexible.

Generally the structures of type I (La_2O_3 and MgO) were selective for oxygenate synthesis, while the structures of type II (TiO_2, ZrO_2, and Al_2O_3) were less selective but more active compared with the type I. A major difference between the [Ru_6C]/MgO, [Ru_6C]/La_2O_3 selective for oxygenate synthesis and the traditional Ru catalysts selective for methane and hydrocarbon formation may be ascribed to the ability of CO dissociation. The amounts of CO adsorbed on the [Ru_6C]/MgO and [Ru_6C]/La_2O_3 at 523 K were as large as eleven or eight CO/cluster, respectively, as shown in Table 3. Particularly on the three Ru atoms of the upper triangle face in the supported cluster in Figure 5, three CO per Ru are likely adsorbed. This situation prevents CO dissociating on the cluster. On the other hand, the structures coordinated with the large amount of CO are disadvantageous for H_2 adsorption. This may be a reason that [Ru_6C]/MgO and [Ru_6C]/La_2O_3 are less active than [Ru_6C]/TiO_2. However, fortunately in view of catalysis, the [Ru_6C] cluster framework is expanded remarkably under the CO/H_2 reaction conditions, which provides the coordination space available for the dissociative adsorption of H_2.[42] In fact the reaction order with respect to H_2 pressure for [Ru_6C]/MgO and [Ru_6C]/La_2O_3 showed a Langmuir-type dependency, while it was about unity (straight line) for [Ru_6C]/TiO_2, suggesting a more facile H_2 adsorption on the former samples at 523 K. These advantageous expansion of the cluster structure made the carbido-cluster catalysts much more active for the oxygenate synthesis compared with the corresponding traditional Ru catalysts in Table 1. Two competitive factors, the number of CO adsorption per cluster and the coordination space for H_2 dissociative adsorption, should make type I selective and type II less selective. These factors are partly affected by the support composition through the cluster structures. It was found that the expanded cluster in P_{CO} = 14.6 kPa was much more active and selective for the oxygenate synthesis than the shrunk cluster in P_{CO} = 0.10 kPa

as shown in Table 2. These results demonstrate the advantageous catalysis of the expanded $[Ru_6C]$/oxide for the oxygenate synthesis from CO/H_2.

The reaction mechanisms via formyl, hydroxycarbene, and formate have been proposed for methanol synthesis.[43] The rate of formate reduction with H_2 was slower than the rate of the steady-state oxygenate synthesis as proved by FT-IR (Table 2), indicating that oxygenate synthesis occurs mainly on Ru_6C entity under the present conditions. Both formyl and hydroxycarbene are known to be thermodynamically unstable.[43-48] The in situ IR observation revealed the presence of a peak at 1576 cm^{-1} (Figure 4) (1551 cm^{-1} in CO/D_2 as listed in Table 7) and this species was very reactive at 523 K. The peak of 1576 cm^{-1} cannot be assigned to hydroxycarbene with a single bonding of carbon and oxygen, but is assignable to the formyl whose end oxygen has interaction with the adjacent Ru atom. The frequency of the formyl peak is compared to the reported values for organometallic formyl complexes in Table 7.

Kellner and Bell reported[49] inverse isotope effects with respect to hydrogen for methane formation in CO/H_2 reaction at 453–543 K with 1.0×10^2 or 1.0×10^3 kPa of CO/H_2 (1:3); r_{CD_4}/r_{CH_4} = 1.4–1.6 on Ru/Al_2O_3. Minor formations of acetaldehyde on Ru/SiO_2 and methanol on Ru/Al_2O_3 also showed inverse isotope effects: $r_{CD_3CDO}/r_{CH_3CHO} \sim 2.0$ and r_{CD_3OD}/r_{CH_3OH} = 1.4–1.6.[50] The oxygenate synthesis on $[Ru_6C]/TiO_2$, $[Ru_6C]/MgO$, and $[Ru_6C]/La_2O_3$ showed inverse isotope effects of 1.4–2.0 as shown in Table 6. The isotope effect in the equilibrium constant for the step, CO(a) + H(a) $\rightleftarrows$ HCO(a), can be calculated on the basis of the vibrational partition functions neglecting the secondary isotope effects.

$$K_D/K_H = \exp[-(CD^{DCO} - CH^{HCO}) - 2(CD^{DCO} - CH^{HCO}) + (s^D - s^H) + (\nu as^D - \nu as^H) + (\delta^D - \delta^H)\}h/(2kT)]$$

Adsorbed hydrogen on $[Ru_6C]$/oxides was considered as μ_2-bridge type with the analogy of a preferable formation of μ_2-bridging hydride in metal–hydride clusters determined by XRD.[30-34] The inverse isotope effect was calculated to be 1.9 by using the reported values for the vibrational modes[23,32,49,51] and the present formyl peak; $\nu_{as(RuHRu)}(Ru_4H_4(CO)_{12})$ = 1585, $\nu_{s(RuHRu)}(Ru_4H_4(CO)_{12})$ = 1290, $\nu_{as(RuDRu)}(Ru_4D_4(CO)_{12})$ = 1153, $\nu_{s(RuDRu)}(Ru_4D_4(CO)_{12})$ = 909, δ_{MH} = 716–810, $\nu_{CH}(Os(CHO)H(CO)_2(PPh_3)_2)$ = 2540, and δ_{CH}(aldehyde) = ~1390 cm^{-1}. The calculated value of 1.9 coincides with the observed value of 1.7 (±0.3). This indicates that the transition state $[CHO]^*$ may be similar to CHO(a) and the step CO(a) + H(a) → CHO(a) may be rate-determining. The rate of H_2–D_2 exchange in the presence of CO was 3000 times larger than the steady-state rate of oxygenate synthesis (Table 2). Therefore, the dissociative adsorption of hydrogen on the carbido cluster should be in equilibrium under CO/H_2 reaction conditions. Accordingly, a catalytic reaction cycle for the oxygenate synthesis on the supported carbido clusters may be shown in Figure 6, where the formyl intermediate is interacted with the neighboring ruthenium atom because μ_1-formyl is unstable thermodynamically[27,43] and also because of the observed red shift of ν_{CO} peak (1576 cm^{-1}). Three oxygenated compounds, methanol, dimethyl ether, and formaldehyde, may be produced via the same intermediate because the three products showed similar hydrogen isotope effects and reaction orders. Dimethyl ether is believed to be formed by the dehydration of methanol on oxide supports.[43]

The formation of hydrocarbons which is more favorable on contracted $[Ru_6C]/TiO_2$ and $/Al_2O_3$ may be initiated by the CO dissociation on the clusters. Negligible isotope effects (ν_D/ν_H ~ 1.0, Table 3) imply that this CO dissociation process would be rate-determining.

The difference of ν_{CO}(main peak) for carbonyls on $[Ru_6C]$/oxides and the corresponding conventional Ru catalysts were as large as 21 cm^{-1} (MgO), 58 cm^{-1} (TiO_2), and 97 cm^{-1} (Al_2O_3) (Table 6), which are larger than general ν_{CO} shifts by the change of Ru particle size in Ru/Al_2O_3.[18] The larger amount of CO adsorbed on Ru would cause a blue shift by a dipole coupling, but this is reverse to the present observation. These ν_{CO} peaks for the $[Ru_6C]$/oxides were observed after the activation at 623 K, but at this temperature the counter cation $[BTMA]^+$ had already been decomposed, excluding the effect of the cation on the peak shift. Thus, the red shift for the supported carbido clusters compared to those for the conventional Ru catalysts may be due to electron donation from the carbido carbon to the ruthenium framework.[7,52,53]

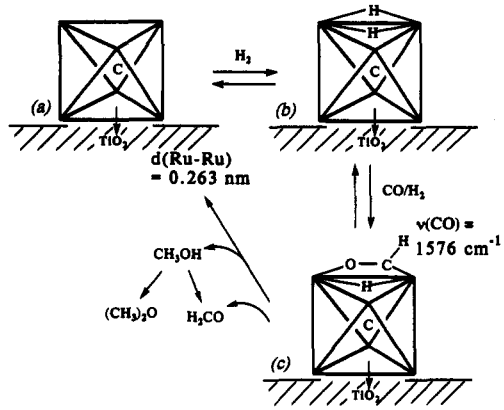

Figure 6. Proposed reaction intermediate for oxygenate synthesis on the TiO_2-supported ruthenium carbido cluster. Carbonyls are not shown to avoid complication of the figure.

Conclusions

1. Supported ruthenium carbido clusters prepared from $[Ru_6C(CO)_{16}(CH_3)]^-$ exhibited selective oxygenate synthesis from CO/H_2 in contrast to the preferential formation of methane and hydrocarbons on supported clusters prepared from $[Ru_6(CO)_{18}]^{2-}$ without interstitial carbido-carbon or on conventional Ru catalysts.

2. Oxygenate-selective $[Ru_6C]/La_2O_3$ and $[Ru_6C]/MgO$ showed reversible expansion–shrink transformation of the $[Ru_6C]$ framework. The $[Ru_6C]$ structure was expanded (d_{Ru-Ru} = 0.277–0.287 nm) under CO/H_2 reaction conditions and shrunk (d_{Ru-Ru} = 0.263 nm) at low CO pressures or in vacuum at 523 K.

3. The expansion of the cluster structure was induced by CO adsorption which is an activated process. The large CO uptake (8–11 CO per cluster) on $[Ru_6C]/MgO$ and $/La_2O_3$ may prevent CO dissociating to increase the selectivity of oxygenate synthesis.

4. The expanded $[Ru_6C]$ structures on MgO and La_2O_3 were more active than the shrunk ones probably due to the larger accessibility of H_2 to dissociatively adsorb on the expanded cluster.

5. $[Ru_6C]/TiO_2$ was most active among the catalysts with the shrunk structure under the reaction conditions.

6. The H_2–D_2 exchange reaction on $[Ru_6C]$/oxides in CO was far faster (>3000 times) than the steady-state oxygenate synthesis. The hydrogen exchange rate on the carbido clusters was larger than that on the traditional Ru catalysts.

7. The inverse isotope effects (ν_D/ν_H) were observed for the oxygenate synthesis on the supported carbido clusters, which can be explained by the zero-point energy in the key step CO(a) + H(a) → HCO(a).

8. The observed peak at 1576 cm^{-1} (1551 cm^{-1}) may be assigned to formyl intermediate.

9. Interstitial carbido carbon is regarded as a central spring for the reversible structure transformation and also as an electron donor to the cluster framework.

References and Notes

(1) *The Chemistry of Metal Cluster Complexes*; Shriver, D. F., Kaesz, H. D., Adams, R. D., Eds.; VCH Publishers: New York, 1990.

(2) Muettertes, E. L.; Krause, M. J. *Angew. Chem., Int. Ed.* Engl. **1983**, *22*, 135.
(3) *Metal Cluster in Catalysis*; Gates, B. C., Guczi, L.; Knözinger, H., Eds.; Elsevier: Amsterdam, 1986.
(4) Lamb, H. H.; Gates, B. C.; Knözinger, H. *Angew. Chem., Int. Ed. Engl.* **1988**, *27*, 1127.
(5) Vargas, M. D.; Nicholls, J. N. *Adv. Inorg. Chem. Radiochem.* **1986**, *30*, 123.
(6) Bradley, J. S. *Adv. Organomet. Chem.* **1983**, *22*, 1.
(7) Halet, J. F.; Evans, D. G.; Mingos, M. P. *J. Am. Chem. Soc.* **1988**, *110*, 87.
(8) Izumi, Y.; Liu, T.; Asakura, K.; Chihara, T.; Yamazaki, H.; Iwasawa, Y. *J. Chem. Soc., Dalton Trans.* **1992**, 2287.
(9) Izumi, Y.; Chihara, T.; Yamazaki, H.; Iwasawa, Y. *J. Chem. Soc., Dalton Trans.*, in press.
(10) Izumi, Y.; Chihara, T.; Yamazaki, H.; Iwasawa, Y. *J. Chem. Soc., Chem. Commun.* **1992**, 1395.
(11) Izumi, Y.; Chihara, T.; Yamazaki, H.; Iwasawa, Y. *J. Am. Chem. Soc.* **1993**, *115*, 6462.
(12) Chihara, T.; Aoki, K.; Yamazaki, H. *J. Organomet. Chem.* **1990**, *383*, 367.
(13) Hayward, C.; Sharpley, J. R. *Inorg. Chem.* **1982**, *21*, 3816.
(14) Eady, C. R.; Jackson, P. F.; Johnson, B. F. G.; Lewis, J.; Malatesta, M. C.; McPartlin, M.; Nelson, W. J. H. *J. Chem. Soc., Dalton Trans.* **1980**, 383.
(15) Teo, B. K., *EXAFS*: *Basic Principles and Data Analysis*; Springer: Berlin, 1986.
(16) Shido, T.; Iwasawa, Y. *J. Catal.* **1990**, *122*, 55.
(17) Binsted, N.; Cook, S. L.; Evans, J.; Greaves, G. N.; Price, R. *J. Am. Chem. Soc.* **1987**, *109*, 3669.
(18) Della Betta, R. A. *J. Phys. Chem.* **1975**, *79*, 2519.
(19) Robbins, J. L. *J. Catal.* **1989**, *115*, 120.
(20) Uchiyama, S.; Gates, B. C. *J. Catal.* **1988**, *110*, 388.
(21) Peirantozzi, R.; Valagene, E. G.; Nordquist, A. F.; Dyer, P. N. *J. Mol. Catal.* **1983**, *21*, 189.
(22) Hertl, W.; Cuenca, A. M. *J. Phys. Chem.* **1973**, *77*, 1120.
(23) Brown, K. L.; Clark, G. R.; Headford, C. E. L.; Marsden, K.; Roper, W. R. *J. Am. Chem. Soc.* **1979**, *101*, 503.
(24) Collins, T. J.; Roper, W. R. *J. Chem. Soc., Chem. Commun.* **1976**, 1044.
(25) Collman, J. P.; Winter, S. R. *J. Am. Chem. Soc.* **1973**, *95*, 4089.
(26) Casey, C. P.; Neumann, S. M. *J. Am. Chem. Soc.* **1976**, *98*, 5395.
(27) Orita, H.; Naito, S.; Tamaru, K. *J. Catal.* **1984**, *90*, 183.
(28) Xiao, F.; Fukuoka, A.; Ichikawa, M. *J. Catal.* **1992**, *138*, 206.
(29) Henderson, M. A.; Worley, S. D. *J. Phys. Chem.* **1985**, *89*, 1417.
(30) Johnson, B. F. G.; Lewis, J.; Williams, I. G. *J. Chem. Soc. A* **1970**, 901.
(31) Chihara, T.; Matsuura, Y.; Yamazaki, H. *J. Chem. Soc., Chem. Commun.* **1988**, 886.
(32) Knox, S. A. R.; Kowpke, J. W.; Andrews, M. A.; Kaesz, H. D. *J. Am. Chem. Soc.* **1975**, *97*, 3942.
(33) Kowpke, J. W.; Johnson, J. R.; Knox, S. A. R.; Kaesz, H. D. *J. Am. Chem. Soc.* **1975**, *97*, 3947.
(34) Johnson, B. F. G.; Lewis, J.; Raithby, P. R.; Süss-Fink, G. *J. Chem. Soc., Dalton Trans.* **1979**, 1356.
(35) Iwasawa, Y. *Catal. Today* **1993**, *18*, 21.
(36) Asakura, K.; Bando, K.; Iwasawa, Y. *J. Chem. Soc., Faraday Trans.* 1990, *86*, 2645.
(37) Asakura, K.; Iwasawa, Y., *J. Chem. Soc., Faraday Trans.* **1990**, *86*, 2657.
(38) Kirlin, P. S.; van Zon, F. B. M.; Koningsberger, D. C.; Gates, B. C. *J. Phys. Chem.* **1990**, *94*, 8439.
(39) Chang, J. R.; Gron, L. U.; Honji, A.; Sanchez, K. M.; Gates, B. C. *J. Phys. Chem.* **1991**, *95*, 9944.
(40) Lamb, H. H.; Gates, B. C. *J. Phys. Chem.* **1992**, *96*, 1099.
(41) Sheu, L. L.; Knözinger, H.; Sachtler, W. H. M. *Catal. Lett.* **1989**, *2*, 129.
(42) Mingos, D. M. P. *Inorg. Chem.* **1982**, *21*, 464.
(43) Klier, K. *Adv. Catal.* **1982**, *31*, 243.
(44) Master, C. *Adv. Organomet. Chem.* **1979**, *17*, 61.
(45) Pacchioni, G.; Fantutti, P.; Koutecký, J.; Ponec, V. *J. Catal.* **1988**, *112*, 34.
(46) Yates, Jr., J. T.; Cavanagh, R. R. *J. Catal.* **1982**, *74*, 97.
(47) Goodman, D. W.; Mafey, T. E.; Ono, M.; Yates, Jr., J. T. *J. Catal.* **1977**, *50*, 279.
(48) Muetterties, E. L.; Stein, J. *Chem. Rev.* **1979**, *79*, 479.
(49) Kellner, C. S.; Bell, A. T. *J. Catal.* **1981**, *67*, 175.
(50) Kellner, C. S.; Bell, A. T. *J. Catal.* **1981**, *71*, 288.
(51) Spectrometric Identification of Organic Compounds, 4th ed.; Silverstein, R. M., Bassler, G. C., Morrill, T. C., Eds.; John Wiley & Sons: New York, 1981.
(52) Ansell, G. B.; Bradley, J. S. *Acta Crystallogr. B* **1980**, *36*, 726.
(53) Mason, R.; Robinson, W. R. *J. Chem. Soc., Chem. Commun.* **1968**, 468.